Contents lists available at ScienceDirect

Autonomic Neuroscience: Basic and Clinical

journal homepage: www.elsevier.com/locate/autneu

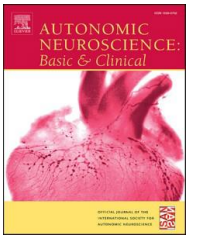

Spectral decomposition of cerebrovascular and cardiovascular interactions in patients prone to postural syncope and healthy controls

Riccardo Pernice[a], Laura Sparacino[a], Vlasta Bari[b], Francesca Gelpi[b,c], Beatrice Cairo[c], Gorana Mijatovic[d], Yuri Antonacci[e], Davide Tonon[f], Gianluca Rossato[f], Michal Javorka[g], Alberto Porta[b,c], Luca Faes[a,*]

[a]*Department of Engineering, University of Palermo, Viale delle Scienze, Bldg. 9, 90128 Palermo, Italy*
[b] *Department of Cardiothoracic, Vascular Anesthesia and Intensive Care, IRCCS Policlinico San Donato, San Donato Milanese, Milan, Italy*
[c] *Department of Biomedical Sciences for Health, University of Milan, Milan, Italy*
[d]*Faculty of Technical Science, University of Novi Sad, Serbia*
[e]*Department of Physics and Chemistry "Emilio Segrè", University of Palermo, Viale delle Scienze, Bldg. 17, 90128 Palermo, Italy*
[f]*Department of Neurology, IRCCS Sacro Cuore Don Calabria Hospital, Negrar, Verona, Italy*
[g]*Department of Physiology and the Biomedical Center Martin, Comenius University in Bratislava, Jessenius Faculty of Medicine, Martin, Slovakia.*

Abstract

We present a framework for the linear parametric analysis of pairwise interactions in bivariate time series in the time and frequency domains, which allows the evaluation of total, causal and instantaneous interactions and connects time- and frequency-domain measures. The framework was applied to physiological time series to investigate the cerebrovascular regulation from the variability of mean cerebral blood flow velocity (CBFV) and mean arterial pressure (MAP), and the cardiovascular regulation from the variability of heart period (HP) and systolic arterial pressure (SAP). Time series were acquired at rest and during the early and late phase of head-up tilt in subjects developing orthostatic syncope in response to prolonged postural stress, and in healthy controls. Spectral measures of total, causal and instantaneous coupling between HP and SAP, and between MAP and CBFV, were integrated in the low-frequency band of the spectrum to analyze specific rhythms, and over all frequencies to get time-domain measures. The analysis of cardiovascular interactions indicated that the postural stress induces baroreflex

* Corresponding author. Tel.: +3909123860236
E-mail address: luca.faes@unipa.it
http://dx.doi.org/10.1016/j. autneu.2021.00.000

Please cite this article as: First author et al., Article title, Autonomic Neuroscience: Basic and Clinical (2021), http://dx.doi.org/10.1016/j.autneu.2021.00.000

involvement, and its prolongation induces baroreflex dysregulation in syncope subjects. The analysis of cerebrovascular interactions indicated that the postural stress enhances the total coupling between MAP and CBFV, and challenges cerebral autoregulation in syncope subjects, while the strong sympathetic activation elicited by prolonged postural stress in healthy controls may determine an increased CBFV→MAP coupling during late tilt. These results document that the combination of time-domain and spectral measures allows to obtain an integrated view of cardiovascular and cerebrovascular regulation in healthy and diseased subjects.

Keywords: cardiovascular control; cerebral autoregulation; autoregressive models; time series analysis; Granger causality; spectral decomposition.

1. Introduction

The cardiovascular and cerebrovascular systems present control mechanisms that maintain physiological variables within acceptable ranges, e.g. in response to variations caused by external stimuli, thus avoiding unsafe values (Cohen and Taylor, 2002). The short-term cardiovascular regulation is carried out by the baroreflex, a mechanism which adjusts the heart period (HP) in response to arterial pressure (AP) changes, limiting excessive AP variability (Cohen and Taylor, 2002; Guyenet, 2006). The arterial baroreflex can be assessed from the spontaneous HP and systolic AP (SAP) variability measuring the simultaneous fluctuations of HP and SAP over time scales up to few hundred beats (Cohen and Taylor, 2002; Krohova et al., 2020; Porta and Elstad, 2020). On the other hand, the short-term cerebrovascular regulation is related to the mechanism of cerebral autoregulation, which has been defined as the intrinsic ability of the brain vessels to independently regulate and thus maintain almost constant the cerebral blood flow (CBF), via changes in cerebrovascular resistance, when mean AP (MAP) fluctuates (Brassard et al., 2021; Zhang et al., 1998a). An extensive study of cerebral autoregulation in humans has been carried out by Lassen (Lassen, 1959), who illustrated the cerebral autoregulation curve and suggested that CBF remains almost constant within a relatively broad mean arterial pressure range (~60-150 mmHg). Moreover, the advent of transcranial doppler ultrasound technology allowed to achieve a temporal resolution sufficient to assess beat-to-beat changes in the CBF velocity (CBFV), and thus to investigate the dynamic properties of cerebral autoregulation (Aaslid et al., 1989).

During orthostatic stress, the CBF may become insufficient due to blood and fluid distending veins and tissues in dependent regions, and to the hydrostatic effect of the difference of height between brain and heart (Claydon and Hainsworth, 2003). In this situation, the two above-described control mechanisms act together to counterbalance this effect: the baroreflex maintains constant or may even increase AP, while the cerebral autoregulation tries to keep the blood flow constant. For this reason, evoking an orthostatic stress, e.g., through head-up tilt test, represents a useful tool to study the baroreflex and the cerebrovascular autoregulation mechanisms, both in healthy conditions and in the presence of autonomic dysfunctions. The proper working of the baroreflex mechanism has been assessed using the measure of baroreflex sensitivity, i.e. the magnitude of HP changes caused by a unit variation of systolic AP (SAP), which has been considered as a marker to predict mortality in particular cohorts of patients, e.g. after myocardial infarction (see e.g. (La Rovere et al., 1998; Nollo et al., 2002; Pernice et al., 2021). Impairment of cardiovascular and/or cerebrovascular regulation has been also related to syncope, i.e. a sudden and brief loss of consciousness associated with a loss of postural tone, usually leading to fainting, but from which recovery is spontaneous (Kapoor, 2000; Martin et al., 2010). In particular, syncope has been associated to baroreflex dysfunction (Béchir et al., 2003) and decrease of cerebral perfusion (Töyry et al., 1997; Van Lieshout et al., 2003). For this reason, several studies have investigated the effects of the impairment of such regulatory mechanisms causing syncope in order to prevent falling by assessing cardiovascular and cerebrovascular variability (Bari et al., 2017; Faes et al., 2005, 2013c; Furlan et al., 2019; Lee et al., 2017; Ocon et al., 2009).

Several approaches have been exploited in the last decades to characterize cardiovascular and cerebrovascular regulations from the spontaneous variability of physiological variables. These approaches range from linear and nonlinear methods (Faes et al., 2019; Giller and Mueller, 2003; Voss et al., 2009) to entropy-based measures of information interaction and decomposition (Faes et al., 2013c; Krohova et al., 2019). In particular, information-theoretic measures allow to quantify the information generated and stored in a process, and the information flow among different coupled processes (Faes et al., 2013c; Krohova et al., 2019). However, the nonlinear and entropy-based analysis of the interactions between processes is typically performed in the time domain and, as such, it accounts for all the oscillations occurring in the whole frequency band, being thus unable to discriminate among different oscillations. This is particularly limiting for cerebrovascular and cardiovascular variability analysis, since there are several concurrent rhythms taking place within different frequency bands. In short-term cardiovascular variability, the most studied rhythms are those occurring at the frequency of the Mayer waves (~0.1 Hz), and those related to respiration, which affects the cardiovascular variables within the high-frequency (HF, 0.15-0.4 Hz) band (Cohen and Taylor, 2002), but can generate confounding effects also in lower frequencies (Krohova et al., 2019; Pernice et al., 2021). With regard to cerebrovascular variability analysis, the main regulatory mechanisms occur within several lower-frequency contiguous bands and for this reason, historically, the most often investigated frequency bands are 0.02–0.07 Hz for the very low frequency (VLF), 0.07-0.2 Hz for the low frequency (LF) and 0.2–0.5 Hz for the high frequency (HF) (Claassen et al., 2016).

For the above-mentioned reasons, it is of great importance to complement the study of cardiovascular and cerebrovascular regulation using tools able to provide spectral profiles for the considered measures of causal and non-causal coupling between time series. This is possible thanks to the use of spectral measures of coupling such as the classical coherence function, and spectral measures of directed (causal) coupling derived from linear parametric autoregressive (AR) models such as the causal coherence and the directed coherence (Faes et al., 2005; Pernice et al., 2021; Porta et al., 2002). However, an issue emerging in the practical analysis of spectral measures of causality is that related to instantaneous effects, i.e. effects from one series to another occurring within the same heartbeat. The classical AR models used to study spectral causality do not incorporate instantaneous effects, which thus remain unexplained as correlations between the model residuals (Faes et al., 2012). While the presence of these effects is accounted in the decomposition of the total time-domain dependence between processes (Geweke, 1982), their spectral interpretation is far less intuitive (Chicharro, 2011). Several approaches have been proposed to account for instantaneous correlations in frequency domain measures, either using extended AR models that incorporate zero-lag effects after determining their direction (Faes et al., 2013a) or keeping them as undirected but including them in "extended" spectral causality measures (Baccalá and Sameshima, 2021; Nuzzi et al., 2021).

In this work, we introduce a framework for the evaluation of total, directed and instantaneous interactions between pairs of time series in both time and frequency domains. The framework is built on previous works establishing a connection between information-theoretic and spectral approaches to the assessment of coupling and causality (Chicharro, 2011; Faes et al., 2021), yielding time domain measures of total coupling, Granger causality and instantaneous interaction that can be retrieved by integrating the corresponding spectral measures over the whole frequency axis. Moreover, the framework is formulated in a way such that two alternative ways are provided to treat instantaneous effects in both time and frequency domains. This is achieved employing traditional and extended linear parametric AR models (Faes et al., 2013a), which are formulated to deal specifically with the beat-to-beat analysis of cerebrovascular interactions probed from CBFV and MAP time series, where instantaneous interactions are typically undirected (Schiatti et al., 2015), and of cardiovascular interactions probed from HP and SAP time series, where directed instantaneous interactions typically describe fast baroreflex effects (Faes et al., 2013a). The framework is employed to study cardiovascular and cerebrovascular interactions in a group of subjects prone to develop orthostatic syncope and in healthy controls in a protocol of prolonged postural stress evoked by head-up tilt testing.

2. Materials and methods

2.1. Measures of linear interaction between stochastic processes

2.1.1. Time domain measures

Let us consider two discrete-time, zero-mean stationary stochastic processes $Y_1(n)$ and $Y_2(n)$, where n is the time index, collected in the bivariate process $\boldsymbol{Y}(n) = [Y_1(n)\ Y_2(n)\ ]^T$. In the linear signal processing framework, the process dynamics can be fully described by the following bivariate autoregressive (AR) model:

$$\boldsymbol{Y}(n) = \sum_{k=1}^{p} \boldsymbol{A}(k)\boldsymbol{Y}(n-k) + \boldsymbol{U}(n), \tag{1}$$

where p is the model order, defining the maximum lag used to quantify interactions, $\boldsymbol{A}(k)$ are 2x2 coefficient matrices defining the time-lagged effects within and between the two scalar processes Y_1 and Y_2 , and $\boldsymbol{U}(n) = [U_1(n)\ U_2(n)]^T$ is a vector of zero-mean *innovation processes* with 2x2 covariance matrix $\boldsymbol{\Sigma} = \mathbb{E}[\boldsymbol{U}(n)\boldsymbol{U}^T(n)] = \begin{bmatrix} \sigma_1^2 & \sigma_{12} \\ \sigma_{21} & \sigma_2^2 \end{bmatrix}$ ($\mathbb{E}[\cdot]$ is the expectation operator). The model (1) is *strictly causal*, meaning that the coefficients contained in $\boldsymbol{A}(k)$ describe only time-lagged interactions occurring for $k > 0$, while *instantaneous interactions*, i.e. interactions occurring at lag zero between the processes, are not described by the model coefficients and thus appear in the off-diagonal elements of the innovation covariance, $\sigma_{12} = \sigma_{21} = \mathbb{E}[U_1(n)\ U_2(n)]$.

To investigate the dynamic interaction between Y_1 and Y_2, restricted models describing the individual dynamics of each single process are introduced. Specifically, the AR model describing the dependence of $Y_i(n), i = 1,2$, on its own past history is formulated as:

$$Y_i(n) = \sum_{k=1}^{\infty} \tilde{a}_i(k) Y_i(n-k) + \tilde{U}_i(n), \tag{2}$$

where the coefficients $\tilde{a}_i(k)$ are generally different from the coefficients $a_{ii}(k)$ contained in the diagonal of $\boldsymbol{A}(k)$, and $\tilde{W}_i(n)$ is a zero mean white noise of variance $\tilde{\sigma}_i^2 = \mathbb{E}[\tilde{U}_i^2(n)]$ which is generally different from the variance σ_i^2 of $U_i(n)$ in (1); note that to capture the full dynamical behavior of Y_i the order of the restricted AR process is infinite even when the original bivariate model has a finite order p (Faes et al., 2017).

Given the model representations reported in (1) and (2), we follow Geweke (Geweke, 1982) to define important measures characterizing the dynamic interactions between the two analyzed processes. Specifically, the total dependence between Y_1 and Y_2 is defined as

$$F_{Y_1,Y_2} = \ln\left(\frac{\tilde{\sigma}_1^2 \tilde{\sigma}_2^2}{|\boldsymbol{\Sigma}|}\right), \tag{3}$$

where $|\cdot|$ denotes the matrix determinant, while the directed interactions from Y_1 to Y_2 and from Y_2 to Y_1 are quantified as

$$F_{Y_1 \to Y_2} = ln\left(\frac{\tilde{\sigma}_2^2}{\sigma_2^2}\right), F_{Y_2 \to Y_1} = ln\left(\frac{\tilde{\sigma}_1^2}{\sigma_1^2}\right); \tag{4}$$

expanding the determinant in (3) and comparing with (4), it is easy to show that the three measures are linked by the decomposition

$$F_{Y_1,Y_2} = F_{Y_1 \to Y_2} + F_{Y_2 \to Y_1} + F_{Y_1 \cdot Y_2}\ , \tag{5}$$

where the last term on the right hand side becomes

$$F_{Y_1 \cdot Y_2} = \ln\left(\frac{\sigma_1^2 \sigma_2^2}{|\boldsymbol{\Sigma}|}\right). \tag{6}$$

The logarithmic measures defined in (3), (4), and (6) are all non-negative, and quantify respectively the total dependence between the two analyzed processes, the causal dependence from one process to another, and the instantaneous interactions between the processes. The measure of total dependence compares the innovations of the full (bivariate) and restricted AR models in a symmetric way, being null when the two processes do not interact (i.e. the $\boldsymbol{A}(k)$ matrices and the innovation covariance matrix $\boldsymbol{\Sigma}$ in (1) are all diagonal) and increasing with the directed and instantaneous interactions in (4) and (5). The measures of directed interaction reflect the principle of Granger causality (Granger, 1969) according to which a process is causal to another if information from the past of the first process helps predicting the present of the second above and beyond the use of its past information only; this principle is quantified in (4) comparing the variance of the innovation processes driving the full and the restricted AR models. Finally, the measure of instantaneous dependence reflects the presence of correlations occurring between the variables that sample the two processes at the same temporal index, being zero when the innovations of the full model are uncorrelated (i.e. when $\sigma_{12} = 0$) and positive otherwise.

Importantly, the measures of dynamic interaction above defined have a clear information-theoretic interpretation in terms of well-known measures such as the mutual information (MI), the MI rate (MIR) and the transfer entropy (TE). In fact, it has been shown that, if the two observed processes have a joint Gaussian distribution, the measure of total coupling given in (3) is two times the MIR, the directed measure of Granger causality given in (4) is two times the TE, and the measure of instantaneous interaction given in (5) is two times the MI between the present state of the two processes conditioned to their past states (Barnett et al., 2009; Chicharro, 2011)].

2.1.2. Frequency domain measures

From the time-domain AR representation of the bivariate process, it is possible to move to the frequency domain through the Fourier transform (FT) of (1), so as to obtain $\boldsymbol{Y}(\bar{f}) = \boldsymbol{H}(\bar{f})\boldsymbol{U}(\bar{f})$, where $\boldsymbol{Y}(\bar{f})$ and $\boldsymbol{U}(\bar{f})$ are the FTs of $\boldsymbol{Y}(n)$ and $\boldsymbol{U}(n)$ and where the 2×2 transfer matrix is $\boldsymbol{H}(\bar{f}) = [\boldsymbol{I} - \boldsymbol{A}(\bar{f})]^{-1} = \overline{\boldsymbol{A}}(\bar{f})^{-1}$, with $\boldsymbol{A}(\bar{f}) = \sum_{k=1}^{p} \boldsymbol{A}(k)e^{-j2\pi\bar{f}k}$; $\bar{f} \in [-0.5,0.5]$ is the normalized angular frequency, $\bar{f} = f/f_s$ (with f_s the sampling frequency), and $\boldsymbol{I}$ is the 2x2 identity matrix. Then, according to an important spectral factorization result, the 2x2 spectral density matrix of the bivariate process can be computed as $\boldsymbol{S}(\bar{f}) = \boldsymbol{H}(\bar{f})\boldsymbol{\Sigma}\boldsymbol{H}^{*}(\bar{f})$, where * stands for the Hermitian transpose; this matrix contains the power spectral density (PSD) of the individual processes, $S_1(\bar{f})$ and $S_2(\bar{f})$, on the diagonal, and the cross-PSDs between the two processes, $S_{12}(\bar{f})$ and $S_{21}(\bar{f}) = S_{12}^{*}(\bar{f})$, out of the diagonal. Given the PSD matrix, it is possible to introduce a spectral measure of total dependence between Y_1 and Y_2 as (Chen et al., 2006)

$$f_{Y_1,Y_2}(\bar{f}) = ln\left(\frac{S_1(\bar{f})S_2(\bar{f})}{|\boldsymbol{S}(\bar{f})|}\right). \tag{7}$$

The measure defined in (7) is important because it is linked to the time-domain measure of total dependence given in (3) by the relation (Chicharro, 2011; Geweke, 1982)

$$F_{Y_1,Y_2} = 2\int_0^{\frac{1}{2}} f_{Y_1,Y_2}(\bar{f})d\bar{f}\,, \tag{8}$$

which evidences how the total coupling between Y_1 and Y_2 can be expanded in the frequency domain, and thus associated to specific oscillations occurring at the same frequency in the two processes.

An expansion similar to (8) holds for the measures of directed interaction defined in (4). In fact, the measures of spectral Granger causality from Y_i to Y_j, defined as (i,j=1,2) (Geweke, 1982)

$$f_{Y_i \to Y_j}(\bar{f}) = ln\,\frac{S_j(\bar{f})}{\sigma_j^2\left|H_{jj}(\bar{f})\right|^2}\,, \tag{9}$$

satisfy the expansion (Chicharro, 2011)

$$F_{Y_i \to Y_j} = 2 \int_0^{\frac{1}{2}} f_{Y_i \to Y_j}(\bar{f}) d\bar{f} \ , \tag{10}$$

thus showing that the time-domain Granger causality measure is retrieved by integrating the spectral measure over the whole frequency axis. Moreover, the spectral measure defined as

$$f_{Y_1 \cdot Y_2}(\bar{f}) \equiv ln \ \frac{\sigma_2^2 \left|H_{22}(\bar{f})\right|^2 \sigma_1^2 \left|H_{11}(\bar{f})\right|^2}{\left|\boldsymbol{S}(\bar{f})\right|} \tag{11}$$

satisfies by construction a decomposition similar to (5), i.e.

$$f_{Y_1,Y_2}(\bar{f}) = f_{Y_1 \to Y_2}(\bar{f}) + f_{Y_2 \to Y_1}(\bar{f}) + f_{Y_1 \cdot Y_2}(\bar{f}) \ , \tag{12}$$

providing the frequency-domain equivalent of the time-domain decomposition of the total coupling between Y_1 and Y_2. Considering the decomposition (5) and the expansions (8) and (10), it is easy to show that the measure (11) appears in the expansion of the time-domain measure of instantaneous interaction (6), i.e.

$$F_{Y_1 \cdot Y_2} = 2 \int_0^{\frac{1}{2}} f_{Y_1 \cdot Y_2}(\bar{f}) d\bar{f} \ ; \tag{13}$$

however, this measure cannot be intended as measuring instantaneous effects between the two processes in the frequency domain, because it can be non-zero even when instantaneous effects are absent (i.e., when $F_{Y_1 \cdot Y_2} = 0$). This also means that $f_{Y_1 \cdot Y_2}$ can take negative values at some frequencies $\bar{f}$, and thus its physical meaning is not straightforward. Since the formulation (11) depends on the two transfer functions H_{12} and H_{21}, and reduces to the time-domain measure (6) when $H_{12}(\bar{f}) = H_{21}(\bar{f}) = 0$, we interpret the spectral measure $f_{Y_1 \cdot Y_2}$ as reflecting a mixing of the directed interactions between Y_1 and Y_2 which contains the effects that cannot be ascribed exclusively to one of the two causal directions. The "mixing effects" can be assessed as redundant at the frequency $\bar{f}$ when the sum of the two directed effects exceeds the total effect, $f_{Y_1,Y_2}(\bar{f}) < f_{Y_1 \to Y_2}(\bar{f}) + f_{Y_2 \to Y_1}(\bar{f}) \Rightarrow f_{Y_1 \cdot Y_2}(\bar{f}) < 0$), and as synergistic when the sum of the two directed effects is lower than the total effect, $f_{Y_1,Y_2}(\bar{f}) > f_{Y_1 \to Y_2}(\bar{f}) + f_{Y_2 \to Y_1}(\bar{f}) \Rightarrow f_{Y_1 \cdot Y_2}(\bar{f}) > 0$.

2.2. Linear interaction measures from parametric models with instantaneous effects

2.2.1. Time domain measures

The strictly causal model introduced in Sect. 2.1 cannot account for instantaneous correlations, i.e. correlations occurring at the same time between the two analyzed processes. In fact, effects between the variables $Y_1(n)$ and $Y_2(n)$ are not described by any coefficient in (1), and are indeed translated into a correlation between the innovations, resulting in a non-diagonal covariance matrix $\boldsymbol{\Sigma}$. As an alternative to (2), the bivariate process $\boldsymbol{Y}(n)$ can be described including instantaneous effects into the interactions allowed by the model (Faes et al., 2013a), leading to the representation

$$\boldsymbol{Y}(n) = \sum_{k=0}^{p} \boldsymbol{B}(k) \boldsymbol{Y}(n-k) + \boldsymbol{W}(n) \, , \tag{14}$$

where the set of coefficients now includes those modeling instantaneous effects collected in the matrix $\boldsymbol{B}(0)$ and $\boldsymbol{W}(n)$ contains the two innovation processes of the extended model. Since instantaneous correlations are now modeled through $\boldsymbol{B}(0)$, the innovations processes have a diagonal covariance matrix $\boldsymbol{\Lambda} = \mathbb{E}[\boldsymbol{W}(n)\boldsymbol{W}^T(n)] = diag\{\lambda_i^2\}$.

The procedure to identify the model (14) is as follows. Knowing $\boldsymbol{B}(0)$, it is possible to compute a so-called mixing matrix $\boldsymbol{L} = [\boldsymbol{I} - \boldsymbol{B}(0)]^{-1}$ and from it to derive the parameters of the extended model (14) from those of the

strictly causal model (1) as $\boldsymbol{B}(k) = \boldsymbol{L}^{-1}\boldsymbol{A}(k)$, $\boldsymbol{\Lambda} = \boldsymbol{L}^{-1}\boldsymbol{\Sigma}(\boldsymbol{L}^{-1})^T$ (Faes et al., 2013a). The matrix of instantaneous effects is obtained solving the instantaneous model $\boldsymbol{U}(n) = \boldsymbol{L}\boldsymbol{W}(n)$ to get the mixing matrix $\boldsymbol{L}$; this task is typically performed imposing a causal order for the instantaneous effects and then following a permutation procedure that involves application of the Cholesky decomposition (Faes et al., 2013a). Here it is important to stress that this approach requires that instantaneous effects are imposed along a given direction (e.g., from $Y_2(n)$ to $Y_1(n)$, allowing $b_{12}(0) \neq 0$) and are neglected along the opposite direction (from $Y_1(n)$ to $Y_2(n)$, forcing $b_{21}(0) = 0$). This condition for identifiability of the extended model implies that the direction of zero-lag effects can be set in a plausible way. Conversely, the extended model (14) cannot be identified unequivocally, and the strictly causal model (1) should be used to model the bivariate process.

Similarly to what observed in Sect. 2.1.1, also for the extended representation it is possible to describe the individual dynamics of each process with simple AR models like those defined in (2). Then, the framework for studying the dependences between the two analyzed processes can be extended to the representation with instantaneous effects. In particular, extended Granger causality measures quantifying the directed interaction between the two processes can be defined as (Schiatti et al., 2015)

$$G_{Y_1 \to Y_2} = ln\left(\frac{\tilde{\sigma}_2^2}{\lambda_2^2}\right), G_{Y_2 \to Y_1} = ln\left(\frac{\tilde{\sigma}_1^2}{\lambda_1^2}\right). \quad (15)$$

In addition, measures of total and instantaneous dependence between Y_1 and Y_2, G_{Y_1,Y_2} and $G_{Y_1 \cdot Y_2}$, can be defined following the reasonings that lead to (3) and (6). The measure of instantaneous dependence is null, i.e. $G_{Y_1 \cdot Y_2} = 0$, because the instantaneous effects are moved to the model coefficients and the innovation covariance is diagonal ($|\boldsymbol{\Lambda}| = \lambda_1^2\lambda_2^2$) (Faes et al., 2013a); moreover, moving the instantaneous effects does not alter the total dependence, i.e. $G_{Y_1,Y_2} = F_{Y_1,Y_2}$, because the determinant of the innovation covariance is preserved ($|\boldsymbol{\Lambda}| = |\boldsymbol{\Sigma}|$). As a consequence, when the bivariate process is represented through an extended AR model, the decomposition of the total dependence simplifies to

$$G_{Y_1,Y_2} = G_{Y_1 \to Y_2} + G_{Y_2 \to Y_1}, \quad (16)$$

which shows how the overall interaction between Y_1 and Y_2 can be expressed as the sum of the causal interactions along the two directions, where the direction $Y_1 \to Y_2$ accounts for both zero-lag and time-lagged effects and the direction $Y_2 \to Y_1$ accounts for time-lagged effects only.

2.2.2. Frequency domain measures

Using the same notations as in Sect. 2.1.2, the frequency-domain representation of the extended model (16) is $\boldsymbol{Y}(\bar{f}) = \boldsymbol{G}(\bar{f})\boldsymbol{W}(\bar{f})$, where $\boldsymbol{G}(\bar{f}) = [\boldsymbol{I} - \boldsymbol{B}(\bar{f})]^{-1}$ and $\boldsymbol{B}(\bar{f}) = \sum_{k=0}^{p} \boldsymbol{B}(k)e^{-j2\pi\bar{f}k}$. From these formulations, the PSD matrix can be written as $\boldsymbol{S}(\bar{f}) = \boldsymbol{G}(\bar{f})\boldsymbol{\Lambda}\boldsymbol{G}^*(\bar{f})$, from which the spectral measure of total dependence between Y_1 and Y_2 takes the same form as in (7), i.e. we have $g_{Y_1,Y_2}(\bar{f}) = f_{Y_1,Y_2}(\bar{f})$. Indeed, the extended representation leads to the same PSDs $S_1(\bar{f})$, $S_2(\bar{f})$, and to the same cross-PSDs $S_{12}(\bar{f})$, $S_{21}(\bar{f})$. The difference with the strictly causal representation stands in how the PSDs are factorized, which leads to different frequency-domain causality measures. Specifically, extended measures of spectral Granger causality from Y_i to Y_j, i,j=1,2, can be defined in analogy to (9) as

$$g_{Y_i \to Y_j}(\bar{f}) = ln\frac{S_j(\bar{f})}{\lambda_j^2\left|G_{jj}(\bar{f})\right|^2}, \quad (17)$$

and an extended spectral measure of the mixing between the two spectral directed interactions can be defined in analogy to (11) as

$$g_{Y_1 \cdot Y_2}(\bar{f}) \equiv ln\frac{\lambda_2^2\left|G_{22}(\bar{f})\right|^2\lambda_1^2\left|G_{11}(\bar{f})\right|^2}{\left|\boldsymbol{S}(\bar{f})\right|}. \quad (18)$$

The measures defined in (17) and (18) satisfy the spectral integration property stated in (10) and (13). Specifically, for the measures of directed interaction we have $G_{Y_i \to Y_j} = 2\int_0^{0.5} g_{Y_i \to Y_j}(\bar{f})d\bar{f}$, which connects the time- and frequency-domain representations of the concept of extended Granger causality; regarding the mixing measure we note that, since $G_{Y_1 \cdot Y_2} = 0$, the spectral integration property indicates that $\int_0^{0.5} g_{Y_1 \cdot Y_2}(\bar{f})d\bar{f} = 0$. Combining (17) and (18) and considering (7), it is easy to show that the decomposition (12) holds also using the extended spectral functions, i.e.

$$g_{Y_1,Y_2}(\bar{f}) = g_{Y_1 \to Y_2}(\bar{f}) + g_{Y_2 \to Y_1}(\bar{f}) + g_{Y_1 \cdot Y_2}(\bar{f}) \ , \tag{19}$$

showing also for the extended representation that the measure defined in (18) provides information about the redundant ($g_{Y_1,Y_2} < g_{Y_1 \to Y_2} + g_{Y_2 \to Y_1} \Leftrightarrow g_{Y_1 \cdot Y_2} < 0$) or synergistic ($g_{Y_1,Y_2} > g_{Y_1 \to Y_2} + g_{Y_2 \to Y_1} \Leftrightarrow g_{Y_1 \cdot Y_2} > 0$) nature of the mixing between the two causal interactions assessed by $g_{Y_1 \cdot Y_2}$.

2.3. Experimental protocol and data analysis

2.3.1. Subjects and experimental protocol

The analyzed data belong to an historical database previously employed to study cardiovascular and cerebrovascular control responses to orthostatic challenge in individuals susceptible to develop postural syncope (Bari et al., 2016; Faes et al., 2013c; Gelpi et al., n.d.). Thirteen subjects (age: 28 ±9 yrs; 5 males) prone to syncope (SYNC) and thirteen age and gender-matched control individuals (nonSYNC, age: 27 ± 8 yrs; 5 males) were analysed in this study. SYNC individuals were subjected to more than three unexplained events of syncope in the previous two years, and the event could be reproduced in laboratory via head-up tilt testing. Subjects were enrolled at the Neurology Division of Sacro Cuore Hospital, Negrar, Italy. Each subject provided informed consent to the experimental protocol, which conformed to the principles of the Declaration of Helsinki for medical research involving humans and was approved by the local Ethical Committee. Before participating to the experiment, subjects avoided drinking caffeine or alcohol-beverage for 24 h, and no individuals of both groups were taking medications affecting cardiovascular control. Head-up tilt test was carried out in a controlled environment, with constant temperature, and subjects laying on a tilt table supported by two belts at the level of thigh and waist, and with feet in contact with the footrest of the table. After laying on the table, the subjects waited for 5 minutes for stabilization of the physiological parameters. Signal acquisition was then carried out for 10 min in the resting supine position, followed by head-up tilt test with tilt table inclination of 60° lasting for maximum 40 min. Prolonged tilt induced signs of vasovagal presyncope in all SYNC subjects with different timings (i.e. progressive hypotension and reflex bradycardia leading to partial loss of consciousness). When these signs were reported, the subject was returned to the resting position and a spontaneous recovery occurred. Conversely, no presyncope signs were reported in any of the nonSYNC subjects. Further details on the experimental protocol can be found in (Bari et al., 2016; Faes et al., 2013c; Gelpi et al., n.d.).

2.3.2. Measurement of physiological time series

The acquired data consisted of surface electrocardiogram (ECG) (lead II), continuous photoplethysmographic AP measured using a volume-clamp device from the middle finger of the right hand (Finapres Ohmeda, Medical Systems, Enschede, The Netherlands) and cerebral blood flow velocity measured from the middle cerebral artery through a transcranial Doppler device (Multi-Dop T, Dwl, 2MHz, Compumedics, San Juan Capistrano, CA, USA). CBFV was investigated in both right and left middle cerebral arteries, but only one signal was then used for obtaining the corresponding time series, on the basis of its quality and signal-to-noise ratio. The signals were acquired synchronously at a sampling rate of 1 kHz.

Cardiovascular and cerebrovascular variability time series were extracted according to the procedure described in the following. A template matching algorithm was employed to detect the QRS complexes and locate the R peaks from ECG signals, in order to calculate HP values as the temporal distance between two consecutive R peaks, i.e. R-

R intervals (Bari et al., 2016). A manual correction procedure was followed to mitigate the effects of ectopic or isolated arrhythmic beats or missing events using linear interpolation between the closest unaffected values (Gelpi et al., n.d.). The *k*-th SAP was defined as the maximum value within the corresponding HP. A low-pass sixth-order Butterworth filter with cut-off frequency of 10 Hz was applied to the CBFV signal. For the analysis of cerebrovascular variability, values of mean AP (MAP) and CBFV were computed respectively integrating the waveform of the sampled pressure and velocity signals within each detected diastolic pulse interval (i.e. the time interval between two consecutive minimum AP values), divided by the duration of the interval itself (Gelpi et al., n.d.). The beat-to-beat variability series of HP, SAP, MAP and mean CBFV, herein referred respectively as *H*, *S*, *M*, and *F*, were then produced as the sequences of consecutive values collected during three stationary time windows of length N=250 beats (Bari et al., 2016; Gelpi et al., n.d.) in the following physiological conditions: (i) supine rest (R); (ii) early tilt (ET), starting after the onset of the head-up tilt maneuver, excluding transient change of the physiological variables; and (iii) late tilt (LT), starting at least 5 minutes after the onset of the head-up tilt maneuver for nonSYNC subjects, or selected as the last stationary window terminating just before the progressive hypotension and reflex bradycardia that mark the beginning of presyncope (16 ± 8 min after the head-up tilt) for SYNC subjects (Faes et al., 2013c).

2.3.3. Data analysis

Standard time-domain statistical parameters such as mean (μ) and variance (σ^2) were computed on the *H*, *S*, *M* and *F* time series measured for each subjects and experimental condition; the corresponding symbols and measurement units are μ_H [ms], σ^2_H [ms^2], μ_S [mmHg], σ^2_S [mmHg^2], μ_M [mmHg], σ^2_M [mmHg^2], μ_F [cm·s^{-1}], and σ^2_F [cm^2·s^{-2}].

The linear interaction measures described in Sections 2.1 and 2.2 were applied to the time series measured for each subject and condition as follows. Each series was first de-trended with an AR high-pass filter with zero phase (cutoff frequency 0.015 cycles/beat) (Nollo et al., 2000). Then, a bivariate AR model was fitted separately on each pair of HP and SAP series to study cardiovascular interactions, and on each pair of MAP and CBFV series to study cerebrovascular interactions. In the first case, the strictly causal model (1) with $Y_1 = M$ and $Y_2 = F$ was used, since the overlap between the time of measurement of the *n*-th MAP sample and the *n*-th CBFV sample did not allow unambiguous setting of instantaneous effects. In the second case, the extended model (14) with $Y_1 = H$ and $Y_2 = S$ was used, allowing - in accordance with the measurement convention depicted in Fig. 1 - the presence of instantaneous effects in the direction from SAP to HP (*i.e.*, setting $b_{12}(0) \neq 0$ and $b_{21}(0) = 0$ as a constraint for model identification), to account for fast (within-beat) baroreflex influences.

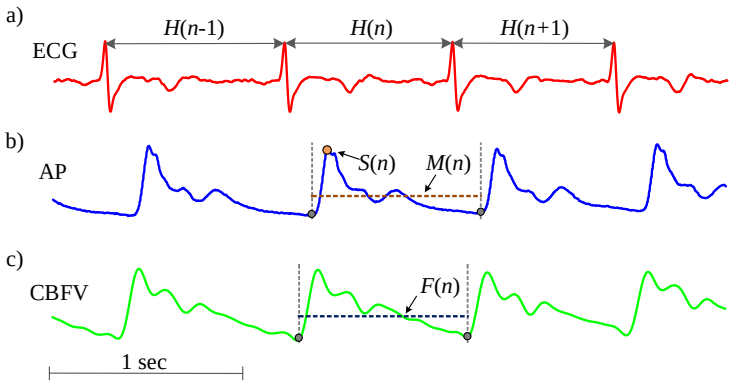

Fig. 1. Measurement of beat-to-beat variability series from exemplary tracings of the ECG, AP and CBFV signals. At the *n*-th cardiac beat, the heart period *H*(*n*) is measured as the ECG R-R interval (a), the SAP value *S*(*n*) and the MAP value *M*(*n*) are measured respectively as the maximum arterial pressure inside *H*(*n*) and as the mean arterial pressure within the diastolic pulse interval related to the cardiac period (b), and the mean CBFV *F*(*n*) is measured as the mean value of the transcranial Doppler ultrasonography signal sampled between its two minima related to the cardiac period (c).

Model identification was performed via the vector least-squares approach, setting the model order p according to the multivariate version of the Akaike Information Criterion (AIC) for each subject (with maximum model order equal to 8) (Akaike, 1974). After AR identification, computation of the time- and frequency-domain interaction measures was performed from the estimated model parameters and spectra of the processes. Spectral analysis was carried out assuming the series as uniformly sampled with the mean heart period ⟨HP⟩ taken as the sampling period, so that the Nyquist frequency in each spectral representation was taken as $\frac{f_S}{2} = \frac{1}{2\langle HP \rangle}$ (Pernice et al., 2021). Frequency-specific measures were obtained integrating the spectral measures within predefined bands. In cardiovascular analysis, the measures were averaged within the low frequency (LF) band of the spectrum (LF, 0.04-0.15 Hz) (Force, 1996) to minimize the effects of non-baroreflex mechanisms on the assessed measures and to avoid the confounding effects of respiration on SAP and HP, which are confined in the high frequency band (Krohova et al., 2019; Pernice et al., 2021; Porta et al., 2002): In cerebrovascular analysis, the measures were averaged within the LF band conventionally adopted for studying MAP-CBFV spectral interactions (0.07-0.2 Hz) (Claassen et al., 2016). An example of time series and computation of the spectral measures for a representative subject is illustrated in Figs. 2 (cardiovascular time series and measures) and 3 (cerebrovascular time series and measures).

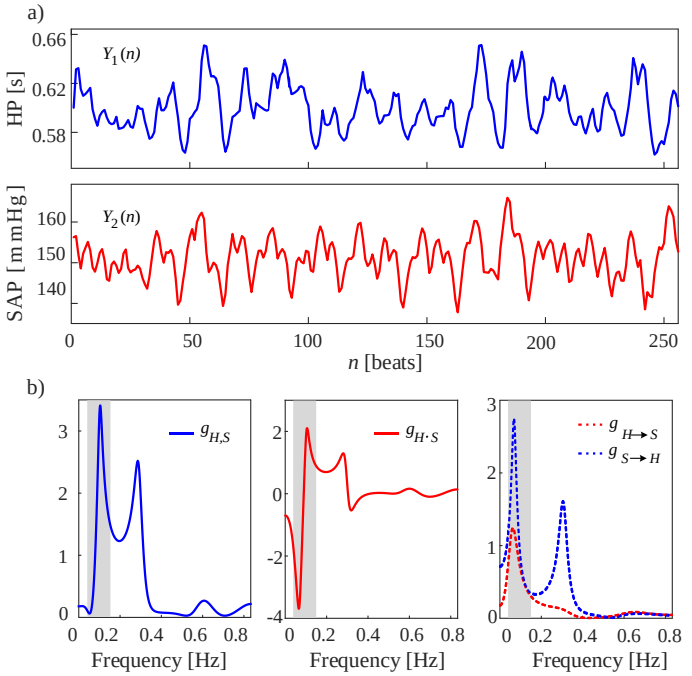

Fig. 2. (a) Example of H and S time series for a representative nonSYNC subject in the late tilt condition; (b) example of frequency domain spectral analysis of baroreflex ($S \rightarrow H$) and feedforward ($H \rightarrow S$) using the extended model; on the left: total linear dependence computed from Eq. (19) (blue continuous line); in the middle: instantaneous term computed from spectral decomposition (Eq. 18); on the right: extended measures of spectral Granger causality along the baroreflex (blue dashed line) and the mechanical feedforward (red dashed line) computed from Eq. 17. Grey area indicates the LF band (0.04-0.15 Hz) used for cardiovascular analysis. For the exemplary subject, model order was p=7, time domain measures: $G_{H,S} = 0.5827$, $G_{H\to S} = 0.1806$, $G_{S\to H} = 0.4026$, $G_{H\cdot S} = 0$; spectral values integrated within the LF band: $g_{H,S}$(LF) $= 1.5287$, $g_{H\to S}$ (LF) $= 0.7525$, $g_{S\to H}$ (LF) $= 1.2103$, $g_{H\cdot S}$ (LF) $= -0.4341$.

2.3.4. Statistical analysis

The distributions of the computed indices were tested for normality using the Anderson-Darling test (Anderson and Darling, 1952; Yap and Sim, 2011). Since the hypothesis of normality was rejected for most distributions, and given the small sample size (Dwivedi et al., 2017), non-parametric tests were employed. For any given group (SYNC and nonSYNC), the non-parametric one-way Friedman test (Cleophas and Zwinderman, 2016) was employed to assess the statistical significance of the differences in the median of the distributions among groups followed, in case of rejection, by a post-hoc pairwise comparison carried out through the paired Wilcoxon non-

parametric test with Bonferroni-Holm correction for multiple comparison (n=3) (Dinno, 2015) to assess the differences between pairs of distributions (R vs ET, R vs LT, ET vs LT). Additionally, the statistical significance of the differences between the two groups (SYNC vs nonSYNC) in a given condition (i.e. rest, early or late tilt) was assessed using the non-parametric Mann-Whitney test. All statistical tests were carried out with 5% significance level.

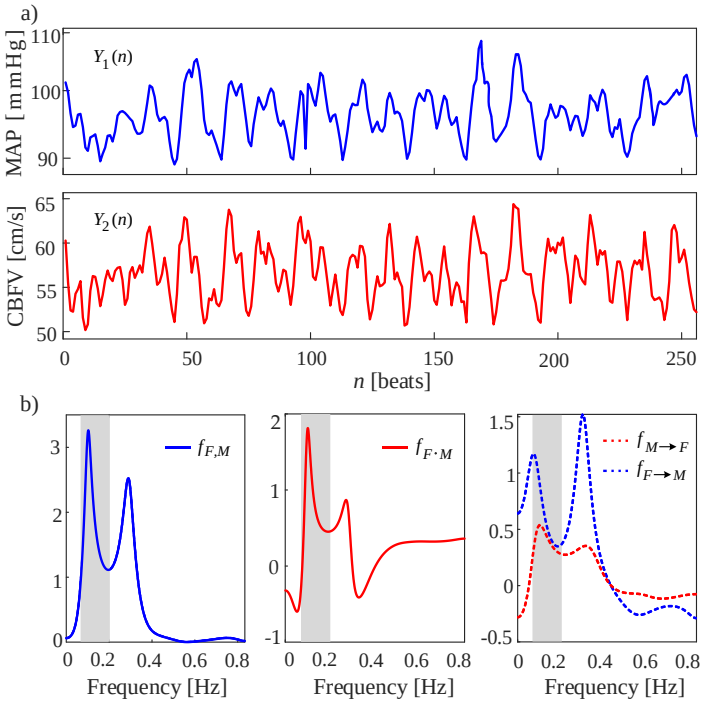

Fig. 3. (a) Example of *M* and *F* time series for a representative nonSYNC subject in the late tilt condition; (b) example of frequency domain spectral analysis using strictly causal model; on the left: total linear dependence computed from Eq. (12); in the middle: instantaneous term computed from Geweke spectral decomposition (Eq. 11); on the right: measures of spectral Granger causality along the flow-to-pressure link (blue dashed line) and the pressure-to-flow link (red dashed line) computed from Eq. (9). Grey area indicates the LF band (0.07-0.2 Hz) used for cerebrovascular analysis. For the exemplary subject, model order was p=7, time domain measures: $F_{M,F} = 0.6439$, $F_{M\to F} = 0.0843$, $F_{F\to \mathrm{M}} = 0.2659$, $F_{M\cdot F} = 0.2937$; spectral values integrated within the LF band: $f_{M,F}(\mathrm{LF}) = 0.3857$, $f_{M\to F}(\mathrm{LF}) = -0.0555$, $f_{F\to \mathrm{M}}(\mathrm{LF}) = 0.9286$, $f_{M\cdot F}(\mathrm{LF}) = -0.4874$.

3. Results

3.1. Cardiovascular variability analysis

Table 1 reports the time-domain statistical parameters, i.e. the mean μ and the variance σ^2, extracted from the HP and SAP series considered in the cardiovascular variability analysis applied to nonSYNC and SYNC subjects during supine rest, early tilt and late tilt conditions. Compared to R, a statistically significant drop of the mean HP was observed during ET and LT in both nonSYNC and SYNC subjects; in SYNC patients there was also a significant decrease of μ_H while comparing ET with LT. In both SYNC and nonSYNC, the mean SAP did not change significantly across conditions. As regards the variability of the two time series, we found significant modifications elicited during tilt in subjects prone to develop orthostatic syncope. Specifically, in SYNC subjects the variance of HP decreased significantly during ET and LT compared to R, and the variance of SAP increased significantly during LT compared with R and with ET. The variance of SAP also increased significantly in nonSYNC controls in both ET and LT compared with R.

Fig. 4 shows the results of the time domain analysis of baroreflex and feedforward interactions between HP and SAP time series, performed for the two groups in the three analyzed conditions. We remark that the time domain measures of total ($G_{H,S}$) and causal ($G_{H\to S}$, $G_{S\to H}$) linear dependence correspond to the equivalent frequency domain measures integrated over the whole frequency axis, and that instantaneous causality is absent ($G_{H\cdot S}=0$) because zero-lag effects are assigned to the direction SAP→HP using the extended AR model. In both groups, the total coupling decreased significantly while moving from LT to ET (Fig. 4a); in SYNC subjects the index was also significantly lower during LT than during R. The decrease in total coupling was mainly determined by a lower interaction along the feedforward direction from HP to SAP, as documented by the significant decrease of $G_{H\to S}$ during LT compared to R in both groups, and during LT compared to ET in nonSYNC subjects (Fig. 4b). In SYNC subjects, the linear interaction along the baroreflex direction from SAP to HP decreased significantly moving from ET to LT (Fig. 4c).

Table 1. Time domain parameters: mean μ and variance σ^2 of H (μ_H, $\sigma^2{}_H$) and S (μ_S, $\sigma^2{}_S$) time series in subjects without history of recurrent postural syncope (nonSYNC), and in subjects with history of recurrent postural syncope (SYNC), during the three phases of the protocol (R, ET and LT conditions). Statistically significant differences (p<0.05): *, R vs. ET and R vs. LT; #, ET vs. LT. No statistically significant differences are detected between groups (nonSYNC vs. SYNC) for a given condition.

	nonSYNC			**SYNC**		
	R	**ET**	**LT**	**R**	**ET**	**LT**
μ_H $[ms]$	848.54 ± 188.26	672.33 ± 107.87 *	672.08 ± 133.39 *	911.07 ± 144.04	740.12 ± 107.73 *	633.95 ± 110.75 * #
σ_H^2 $[ms^2]$	1793.76 ± 1732.49	1311.33 ± 1021.69	891.43 ± 474.46	3124.11 ± 2897.07	1692.62 ± 1468.53 *	1103.08 ± 1167.54 *
μ_S $[mmHg]$	140.02 ± 28.05	136.08 ± 17.90	128.82 ± 16.81	125.10 ± 21.41	138.52 ± 23.016	127.34 ± 23.32
$\sigma_S^2[mmHg^2]$	19.54 ± 13.50	30.95 ± 24.96 *	31.79 ± 21.59 *	18.40 ± 16.86	26.54 ± 13.36	35.26 ± 16.60 * #

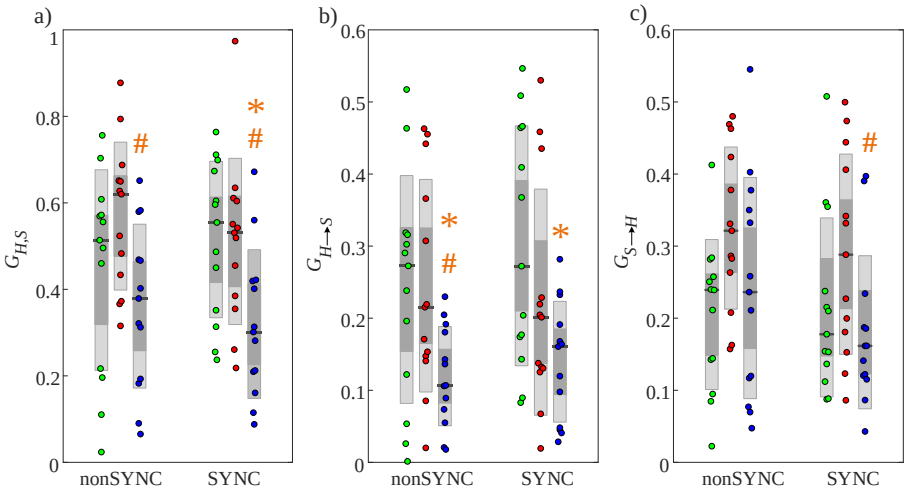

Fig. 4. Time-domain analysis of cardiovascular interactions. Plots depict the distributions across subjects, shown as individual values and box-plot distributions, of the total linear interaction between HP and SAP (a), and of the directed interaction from HP to SAP (b) and from SAP to HP (c), computed at rest (R, left bars and green circles) and during head-up tilt (ET, middle bars and red circles; LT, right bars and blue circles). Statistically significant differences: *, R vs. ET and R vs. LT; #, ET vs. LT. No statistically significant differences are detected between groups (nonSYNC vs. SYNC) for a given condition.

The results of the frequency domain analysis of cardiovascular interactions are reported in Fig. 5. All spectral measures were averaged within the LF band of the spectrum, quantifying the total information shared in this band between HP and SAP ($g_{H,S}$(LF)), the information transferred along the two causal directions ($g_{H\to S}$(LF), $g_{S\to H}$(LF)), and the information related to the mixing between the two directions ($g_{H\cdot S}$(LF)). The significant changes observed in the total coupling measure integrated over all frequencies (Fig. 4a) were observed when focusing on the LF band only for the nonSYNC subjects, for which the measure $g_{H,S}$(LF) increased significantly moving from R to ET, and

decreased significantly moving from ET to LT; the measure did not change significantly in SYNC subjects (Fig. 5a). These trends are mainly linked to the modifications of the mixing term $g_{H\cdot S}$(LF), which indeed increased from R to ET and decreased from ET to LT in nonSYNC subjects but not in SYNC subjects (Fig. 5c). The linear interaction from HP to SAP showed a tendency to decrease progressively moving from R to ET and LT, but the decrease was statistically significant only comparing LT and R in SYNC subjects (Fig. 5b). On the contrary, the linear interaction from SAP to HP increased markedly while moving from R to ET in both groups, and moving from ET to LT in SYNC (Fig. 5d).

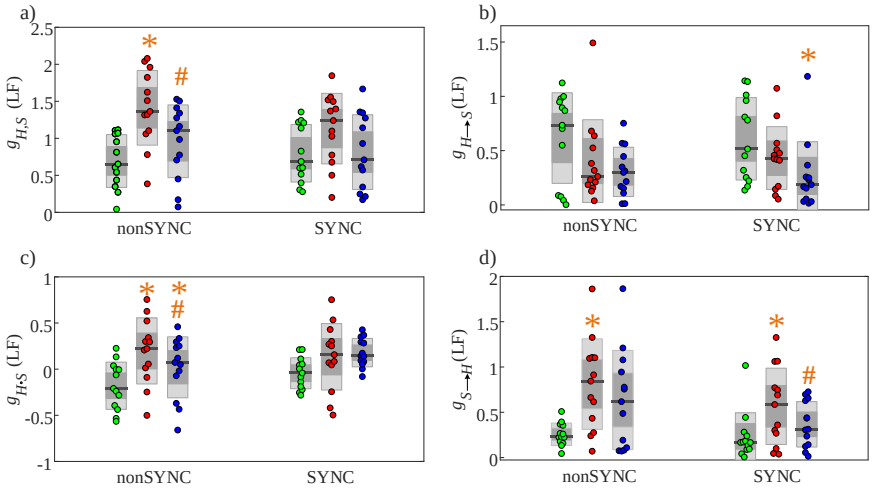

Fig. 5. Frequency-domain analysis of cardiovascular interactions performed integrating the spectral measures within the low frequency band (LF, 0.04-0.15 Hz). Plots depict the distributions across subjects, shown as individual values and box-plot distributions, of the LF values obtained for the total linear interaction between HP and SAP (a), the directed interaction from HP to SAP (b), the mixing between the two interactions (c), and the directed interaction from SAP to HP (d), computed at rest (R, left bars and green circles) and during head-up tilt (ET, middle bars and red circles; LT, right bars and blue circles). Statistically significant differences: *, R vs. ET and R vs. LT; #, ET vs. LT. No statistically significant differences are detected between groups (nonSYNC vs. SYNC) for a given condition.

3.2. Cerebrovascular variability analysis

Table 2 reports the time domain parameters (mean μ and variance σ^2) extracted from the MAP and CBFV cerebrovascular series. The mean values of the MAP series were significantly higher during ET and LT compared to R in the SYNC subjects, while they did not change significantly in nonSYNC. The mean CBFV decreased significantly during the tilt epochs in both groups; while in nonSYNC subjects ET and LT were comparable, in SYNC subjects the decrease was progressive from R to ET to LT. The variance of the two series did not change significantly across conditions or between groups.

Table 2. Time domain parameters: mean μ and variance σ^2 of M (μ_M, ${\sigma^2}_M$) and F (μ_F , ${\sigma^2}_F$) time series in nonSYNC, group without history of recurrent postural syncope, and SYNC, group with history of recurrent postural syncope, during the three phases of the protocol (R, ET and LT conditions). Statistically significant differences (p<0.05): *, R vs. ET and R vs. LT; x, ET vs. LT. No statistically significant differences are detected between groups (nonSYNC vs. SYNC) for a given condition.

	nonSYNC			**SYNC**		
	R	ET	**LT**	**R**	**ET**	**LT**
$\boldsymbol{\mu_M\ [mmHg]}$	98.84 ± 17.33	95.16 ± 12.17	92.94 ± 11.61	84.42 ± 13.96	97.16 ± 17.50 *	93.53 ± 15.64 *
$\boldsymbol{\sigma_M^2\ [mmHg^2]}$	14.22 ± 14.79	15.38 ± 9.11	14.56 ± 9.46	9.08 ± 6.78	13.61 ± 7.26	15.08 ± 6.99
$\boldsymbol{\mu_F\ [cm\cdot s^{-1}]}$	72.02 ± 23.14	62.12 ± 21.52 *	61.09 ± 15.72 *	64.42 ± 17.25	56.25 ± 17.06 *	48.12 ± 18.06 * #
$\boldsymbol{\sigma_F^2[cm^2\cdot s^{-2}]}$	12.74 ± 8.20	20.42 ± 11.42 *	15.42 ± 10.38	34.67 ± 72.69	41.56 ± 95.99	32.20 ± 56.31

The results of time domain analysis of cerebrovascular interactions are depicted in Fig. 6. Besides the measures of total ($F_{M,F}$) and causal ($F_{M\to F}$, $F_{F\to M}$) linear dependence between MAP and CBFV, the figure reports also the measure of instantaneous interaction $F_{M\cdot F}$, which is nonzero in this case where the strictly causal AR model was adopted to fit the time series (Fig. 6c). The total dependence between the two series showed a tendency to increase with tilt (Fig. 6a); the increase was statistically significant only for the SYNC subjects during ET. This tendency was supported in SYNC subjects by the significant increase of the linear interaction from MAP to CBFV during ET and LT compared to R (Fig. 6b), while the linear interaction along the opposite causal direction (Fig. 6d) and the instantaneous interaction were substantially unaffected by tilt (Fig. 6c). In nonSYNC subjects, a tendency towards higher values of linear coupling from CBFV to MAP was observed (Fig. 6d), with significantly higher values of $F_{F\to M}$ during LT compared to R; the coupling from MAP to CBFV and the instantaneous coupling did not change across conditions in this group (Fig. 6b).

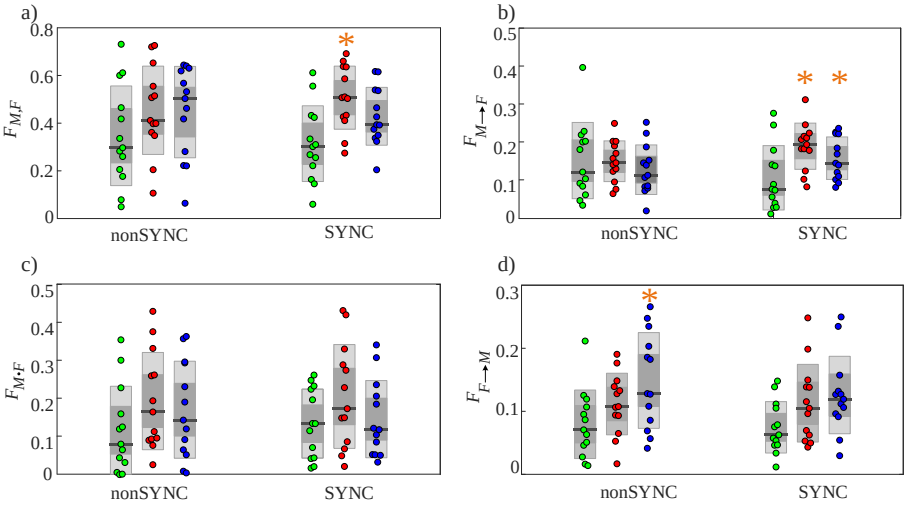

Fig. 6. Time-domain analysis of cerebrovascular interactions. Plots depict the distributions across subjects, shown as individual values and box-plot distributions, of the total linear interaction between CBFV and MAP (a), the directed interaction from MAP to CBFV (b), the instantaneous interaction between CBFV and MAP (c), and the directed interaction from CBFV to MAP (d), computed at rest (R, left bars and green circles) and during head-up tilt (ET, middle bars and red circles; LT, right bars and blue circles). Statistically significant differences: *, R vs. ET and R vs. LT; #, ET vs. LT. No statistically significant differences are detected between groups (nonSYNC vs. SYNC) for a given condition.

The results of the frequency domain analysis of cerebrovascular interactions are reported in Fig. 7. The spectral measures were averaged within the LF band of the spectrum, quantifying the total information shared in this band between CBFV and MAP ($f_{M,F}(\mathrm{LF})$), the information transferred along the two causal directions ($f_{M\to F}(\mathrm{LF})$, $f_{F\to M}(\mathrm{LF})$, which can be negative in some cases), and the information related to the mixing between the two directions ($f_{M\cdot F}(\mathrm{LF})$). When assessed within the LF band, the total coupling (Fig. 7a) exhibits the same behaviour in the two groups, i.e. a significant increase during both ET and LT compared to R; in the time domain, such an increase was reported only in SYNC individuals during ET (Fig. 6a). The increased cerebrovascular coupling during tilt was reflected in its most part by the measure quantifying mixing and instantaneous effects (Fig. 7c), as documented by the significantly higher values observed for $f_{M\cdot F}(\mathrm{LF})$ during LT in nonSYNC subjects and during both ET and LT in SYNC subjects. A statistically significant increase is also detected during LT for the linear interaction from CBFV to MAP in nonSYNC subjects (Fig. 7d), and during LT for the linear interaction from MAP to CBFV in SYNC subjects (Fig. 7b).

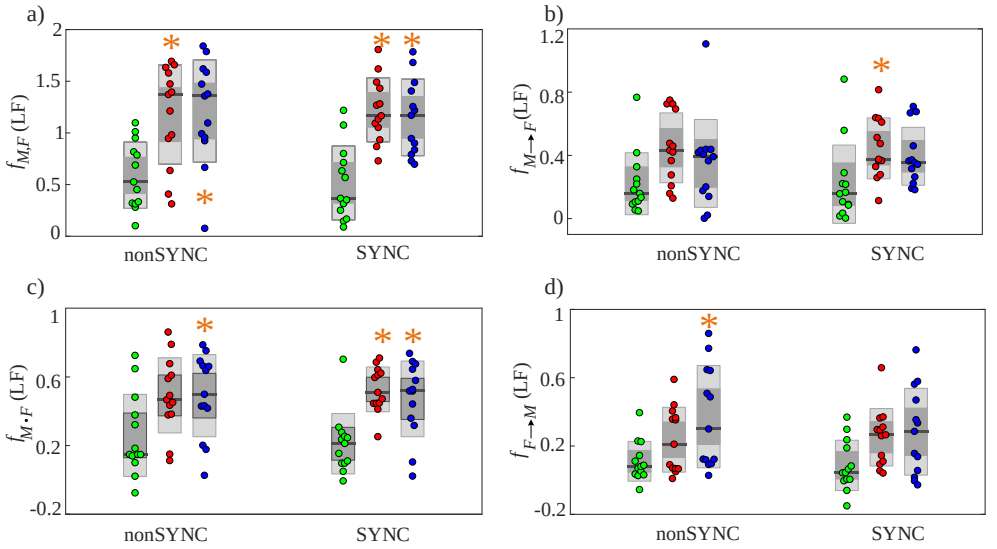

Fig. 7. Frequency-domain analysis of cerebrovascular interactions performed integrating the spectral measures within the low frequency band (LF, 0.07-0.2 Hz). Plots depict the distributions across subjects, shown as individual values and box-plot distributions, of the LF values obtained for the total linear interaction between CBFV and MAP (a), the directed interaction from MAP to CBFV (b), the mixing and instantaneous interaction between the two directions (c), and the directed interaction from CBFV to MAP (d), computed at rest (R, left bars and green circles) and during head-up tilt (ET, middle bars and red circles; LT, right bars and blue circles). Statistically significant differences: *, R vs. ET and R vs. LT; #, ET vs. LT. No statistically significant differences are detected between groups (nonSYNC vs. SYNC) for a given condition.

4. Discussion

The main findings of this work, which are discussed in detail in Sections 4.1 and 4.2, can be summarized as follows:

- The evaluation of coupling and causality measures within confined frequency bands related to well-defined physiological oscillations allows to highlight behaviours related pathophysiological mechanisms which are otherwise often hidden in time-domain measures reflecting whole-band interactions.
- The short-term cardiovascular regulation is enhanced by head-up tilt as a result of a larger baroreflex involvement, and is weakened by prolongation of the postural stress, as a result of decreased mechanical effects and, in syncope subjects, of an autonomic dysregulation possibly related to baroreflex impairment.
- The cerebrovascular response to postural stress is reflected by an increased coupling between MAP and CBFV, which becomes evident when focusing on LF oscillations (0.07-0.2 Hz) and is determined by a synergistic effect of the two causal pathways forming the pressure-flow bidirectional interaction.
- The directed coupling from MAP to CBFV increased significantly during early head-up tilt in syncope subjects but not in healthy controls, suggesting that the postural stress challenges cerebral autoregulation in subjects prone to syncope development.
- The directed coupling from CBFV to MAP increased significantly during late head-up tilt in healthy controls but not in syncope subjects, suggesting that the strong activation of the sympathetic system elicited by prolonged postural stress may also enhance the observed causal coupling indirectly through its effects on CBFV and on MAP.

4.1. Cardiovascular variability analysis

The variations observed across conditions for the standard time-domain statistics (Table 1) reflect physiologically explainable changes which are expected as a consequence of the orthostatic stress. In particular, the significant i of the increase of heart rate (lower μ_H) and the increase of the SAP variability (higher σ_S^2) observed in both groups

during head-up tilt reflect the vagal withdrawal and sympathetic activation generated by the orthostatic stress and are driven by the baroreflex response resulting from the blood pressure decrease associated with a drop of central blood volume (Furlan et al., 2000; Montano et al., 1994; Porta et al., 2007). Moreover, the further significant modifications of these parameters observed during LT highlight the impending dysregulation of the cardiovascular function before presyncope, characterized by stronger tachycardia and elevated blood pressure variability (Furlan et al., 2019).

With regard to the time-domain analysis of baroreflex and feedforward interactions based on the considered measures of linear dependence, the two groups behaved rather similarly in their response to postural stress, showing a significant reduction of the total coupling between HP and SAP during late tilt (Fig. 4). This result indicates that the prolongation of the orthostatic stress produces an overall weakening of the closed-loop cardiovascular regulation. The decomposition into measures of directed interaction evidenced that the drop is related to the HP→SAP direction in both groups, and also to the SAP→HP direction in the subjects prone to orthostatic syncope. On the other hand, the time-domain analysis did not document an increase of coupling between SAP and HP moving from the resting supine position to the upright position during ET. Such an increase, which is expected from the results of a number of previous studies documenting a larger involvement of the baroreflex into the cardiovascular regulation exerted during postural stress (Cooke et al., 1999; Faes et al., 2013b; Porta et al., 2011), was observed in our work in the trends of the frequency-domain measures of total coupling, mixing and directed coupling from SAP to RR computed within the LF band of the spectrum (Fig. 5). In previous studies, it has been related to an increased involvement of the baroreflex into cardiovascular regulation consequent to the postural stress (Cooke et al., 1999; Faes et al., 2013b; Porta et al., 2011). The fact that this behavior becomes evident only looking at the LF band can be explained by the role played by respiration, which affects both SAP and HP acting mostly in the high-frequency band (0.15-0.4 Hz) and may act as a confounder of cardiovascular interactions assessed through time-domain measures accounting for the whole frequency spectrum (Porta et al., 2012, 2002).

The main differentiation between the two analyzed groups consisted in the decreased interaction along the feedback direction from SAP to HP observed in syncope subjects but not in healthy controls. This result was documented both by the time domain analysis (Fig. 4c) and by the spectral analysis restricted to the LF band (Fig. 5d), and suggests an impairment of the baroreflex control as a symptom of autonomic dysfunction preceding postural syncope. This interpretation is in agreement with previous studies indicating that the diminished baroreflex involvement could be one of the main mechanisms responsible for the impairment of the cardiovascular control associated with syncope development (Mosqueda-Garcia et al., 1997; Nollo et al., 2009). A similar drop of the coupling strength along the baroreflex has been detected previously in spontaneous cardiovascular variability analyses using both nonlinear information-based techniques (Faes et al., 2013b, 2013c) and linear approaches computing the directed coherence in the frequency domain (Faes et al., 2005).

The linear interaction from HP to SAP decreased moving from rest to tilt and with prolongation of the postural stress (Figs. 4b and 5b). This result suggests that feedforward effects, which comprise cardiac autoregulation (e.g., the Frank–Starling law) and previously described HP→diastolic arterial pressure→SAP sequence (Javorka et al., 2017; Porta and Faes, 2013), tend to decrease progressively their contribution to the cardiovascular regulation when the orthostatic challenge intensifies. Finally, the term reflecting the mixing between feedback and feedforward interactions, evaluated in the LF band of the spectrum, increased with the transition from rest to tilt; the variation was statistically significant only for the healthy controls (Fig. 5c). As this term measures the balance between redundant and synergistic interactions along the two causal directions, the observed increase suggests that the feedback and feedforward arms of the cardiovascular closed-loop explain a lower part of the total interactions between the LF oscillations of SAP and HP during tilt than in the resting condition.

4.2. Cerebrovascular variability analysis

The variations observed across conditions for the time-domain statistics (Table 2) reflect mechanisms related to postural stress and orthostatic intolerance. The reduction of mean CBFV during tilt in both groups is in agreement with previous studies demonstrating a mild drop of CBFV in response to orthostatic challenge (Novak, 2016), and has been related to cerebral vasoconstriction probably associated with an augmented sympathetic nerve activity during lower body negative pressure (LBNP) (Levine et al., 1994; Silvani et al., 2003; Zhang et al., 1998b). The

CBFV decrease is even more marked in SYNC patients, likely being the consequence of the so-called "paradoxical cerebral vasoconstriction" during tilt contributing to orthostatic vasovagal reactions in patients with presyncope (Dan et al., 2002; Grubb et al., 1991; Silvani et al., 2003). In SYNC patients, the increase of the mean MAP values during ET and LT and the progressive reduction of CBFV from R to ET and to LT may be related to an impaired cerebrovascular autoregulation before the onset of presyncope signs, as previously reported in (Faes et al., 2013c).

The time-domain analysis of the pressure-to-flow interactions reported in Fig. 6b documented that, while no significant changes of the directed coupling from MAP to CBFV were detected in healthy controls, the measure increased significantly during both tilt epochs in the syncope patients. The same trends were observed when the directed interaction from MAP to CBFV was computed within the LF band (0.07-0.2 Hz), documenting that the effect is relevant to this portion of the frequency spectrum (Fig. 7b). The increase of MAP→CBFV causal interactions in SYNC subjects suggests that the cerebrovascular autoregulation mechanisms may be impaired during tilt in this group. Indeed, cerebral autoregulation aims at maintaining mean CBFV relatively constant in presence of modifications of mean arterial pressure (Aaslid et al., 1989; Paulson et al., 1990), thus attempting to preserve a certain degree of uncoupling between mean CBFV and MAP in a range of values of MAP as wide as possible. Accordingly, an increased causal coupling from MAP to CBFV may be interpreted as an indication of a less effective or impaired cerebrovascular autoregulation (Panerai et al., 1998; Zhang et al., 1998a). This result is in line with previous findings using Granger causality measures (Schiatti et al., 2015) and transfer entropy measures (Bari et al., 2017; Faes et al., 2013c) suggesting that the postural challenge reduces the effectiveness of the cerebrovascular control in patients prone to postural syncope.

Looking at the interactions along the causal direction from CBFV to MAP, the coupling strength shows a tendency to increase progressively during postural stress; this tendency was statistically significant only in nonSYNC subjects after prolonged stress (Fig. 6d). The same trends were observed when the directed interaction from CBFV to MAP was computed within the LF band (0.07-0.2 Hz), documenting that the effect is relevant to this portion of the frequency spectrum (Fig. 7d). The physiological interpretation of such results is challenging, also given that the mechanisms of cerebrovascular regulation are still not completely understood and likely differ with pressure variations (Cipolla, 2009). Even though the influence of sympathetic activity on cerebral blood flow has been debated in the literature and often considered negligible under normal conditions (van Lieshout and Secher, 2008), under very high or very low blood pressure conditions the sympathetic perivascular nerves which innerve cerebral arteries may be activated to constrict the inflow tract cerebral vessels (van Lieshout and Secher, 2008). As a consequence, we may speculate that the sympathetic activity enhances the observed causal coupling through its effects on CBFV and on MAP, according to the Cushing reflex (Saleem et al., 2018). Although the Cushing mechanism has been traditionally described in agonic situations as a last resort to prevent brain hypoperfusion by increasing blood pressure above the intracranial pressure level possibly augmented due to, for example, cerebral haemorrhage, support for the intervention of this mechanism in more physiological and less critical situations has been reported as well (Bari et al., 2017; Dickinson and McCubbin, 1963; McBryde et al., 2017; Shanlin et al., 1988). However, the possibility that the relevance of the link from CBFV to MAP could be augmented as a mere consequence of unaccounted confounding factors could not be completely dismissed without interventions manipulating CBF or at least able to modify determinants of this pathway, for example by alpha-adrenergic blockade. These findings should be anyway confirmed in larger datasets, also because the same enhancement of the information transfer from CBFV to MAP was not clearly documented in previous studies (Bari et al., 2017; Schiatti et al., 2015). The differences may be due to the adopted methodology ((Bari et al., 2017) employed transfer entropy, and (Schiatti et al., 2015) assigned instantaneous causality to the causal measure) and the difference in the protocols ((Bari et al., 2017) did not distinguish the tilt epochs, and (Schiatti et al., 2015) did not consider healthy controls).

The comparison between time-domain measures accounting for whole-band interactions and frequency-specific measures computed within the LF band (0.07-0.2 Hz) indicates that the measures of directed interaction behaved similarly (Fig. 6b,d vs. Fig. 7b,d), whereas the measures of total coupling and mixing exhibited different patterns in response to orthostatic stress (Fig. 6a,c vs. Fig. 7a,c). In fact, while the time-domain measures did not evidence marked changes across conditions, the LF measures of total coupling and mixing displayed marked and statistically significant increments during the postural stress. This indicates that instantaneous effects between CBFV and MAP play an important role in cerebrovascular interactions and may confound -together with interactions occurring outside the LF band- the detection of the impact of the postural challenge on cerebral autoregulation. We remark

that, according to our results, this impact is the same in SYNC and nonSYNC subjects when it is assessed in terms of measures that account for both pathways of the bidirectional interaction between MAP and CBFV; the differences between the two groups emerged considering the causal measures as discussed above.

4.3. Limitations and future developments

In our statistical analyses, no differences between the two analyzed groups of SYNC and nonSYNC subjects were detected. While this result may suggest that any modification of the cardiovascular or cerebrovascular control in patients prone to develop syncope is better detectable observing the response to the orthostatic challenge rather than comparing different groups, it may be a consequence of the small dataset analyzed. A main limitation of the present study concerns indeed the small number of subjects involved, which may affect the robustness of the obtained results. Future studies involving more participants should be performed to confirm the results and corroborate the interpretations of the current study.

From a methodological point of view, although our work provides an integrated framework to assess total and causal interactions in bivariate time series in both time and frequency domains, it does not provide conclusive information about the treatment of instantaneous interactions in the computation of the presented measures. Here, instantaneous interactions were assigned to a specific causal direction based on physiological knowledge in the cardiovascular analysis, and were left unassigned in the absence of such knowledge in the cerebrovascular analysis. Alternative approaches have been explored, including the use of non-Gaussian modelling and independent component analysis to set the direction of instantaneous effects without prior knowledge (Faes et al., 2013c; Schiatti et al., 2015), and the use of disconnected AR models studied in the frequency domain to provide undirected measures of instantaneous causality and extended measures of Granger causality (Nuzzi et al., 2021). Since our work confirms that instantaneous effects play a fundamental role in cardiovascular and cerebrovascular variability analysis, future studies are envisaged to compare our framework with existing approaches, to assess the agreement of these methods in the evaluation of frequency-domain interaction and shed more light on this delicate issue.

5. Conclusion

The present work introduced a unified framework for the analysis of pairwise interactions between time series, decomposing the overall interaction into directed and instantaneous effects and considering both time- and frequency-domain representations. The added value of the framework stands in the tight relation between the measures defined in the time and frequency domains, which favors interpretability, and in the possibility to incorporate instantaneous influences into one causal direction or leave them isolated in the evaluation of the interactions, which brings flexibility. Exploiting these features, we contributed to describe the physiological mechanisms involved in the cardiovascular and cerebrovascular regulation in the response to a physiological stimulation (i.e., the postural stress) and to the development of an autonomic dysfunction (i.e., the pre-symptoms of postural related syncope). In perspective, the combination of time- and frequency-domain measures can help elucidating the mechanisms behind the oscillatory rhythms as well as the broadband dynamics of coupled physiological variables studied in a variety of physiological conditions and diseased states.

Acknowledgments

R.P. is supported by the Italian MIUR PON R&I 2014-2020 AIM project no. AIM1851228-2. L.F. is supported by the Italian MIUR PRIN 2017 project 2017WZFTZP “Stochastic forecasting in complex systems”.

References

Aaslid, R., Lindegaard, K.-F., Sorteberg, W., Nornes, H., 1989. Cerebral autoregulation dynamics in humans. Stroke 20, 45–52.

Anderson, T.W., Darling, D.A., 1952. Asymptotic theory of certain" goodness of fit" criteria based on stochastic

processes. Ann. Math. Stat. 23, 193–212.
Baccalá, L.A., Sameshima, K., 2021. Frequency Domain Repercussions of Instantaneous Granger Causality. Entropy 23, 1037.
Bari, V., De Maria, B., Mazzucco, C.E., Rossato, G., Tonon, D., Nollo, G., Faes, L., Porta, A., 2017. Cerebrovascular and cardiovascular variability interactions investigated through conditional joint transfer entropy in subjects prone to postural syncope. Physiol. Meas. 38, 976.
Bari, V., Marchi, A., De Maria, B., Rossato, G., Nollo, G., Faes, L., Porta, A., 2016. Nonlinear effects of respiration on the crosstalk between cardiovascular and cerebrovascular control systems. Philos. Trans. R. Soc. A Math. Phys. Eng. Sci. 374, 20150179.
Barnett, L., Barrett, A.B., Seth, A.K., 2009. Granger causality and transfer entropy are equivalent for Gaussian variables. Phys. Rev. Lett. 103, 238701.
Béchir, M., Binggeli, C., Corti, R., Chenevard, R., Spieker, L., Ruschitzka, F., Lüscher, T.F., Noll, G., 2003. Dysfunctional baroreflex regulation of sympathetic nerve activity in patients with vasovagal syncope. Circulation 107, 1620–1625.
Brassard, P., Labrecque, L., Smirl, J.D., Tymko, M.M., Caldwell, H.G., Hoiland, R.L., Lucas, S.J.E., Denault, A.Y., Couture, E.J., Ainslie, P.N., 2021. Losing the dogmatic view of cerebral autoregulation. Physiol. Rep. 9, e14982.
Chen, Y., Bressler, S.L., Ding, M., 2006. Frequency decomposition of conditional Granger causality and application to multivariate neural field potential data. J. Neurosci. Methods 150, 228–237.
Chicharro, D., 2011. On the spectral formulation of Granger causality. Biol. Cybern. 105, 331–347.
Cipolla, M.J., 2009. Control of cerebral blood flow, in: The Cerebral Circulation. Morgan & Claypool Life Sciences.
Claassen, J.A.H.R., Meel-van den Abeelen, A.S.S., Simpson, D.M., Panerai, R.B., (CARNet), I.C.A.R.N., 2016. Transfer function analysis of dynamic cerebral autoregulation: A white paper from the International Cerebral Autoregulation Research Network. J. Cereb. Blood Flow Metab. 36, 665–680.
Claydon, V.E., Hainsworth, R., 2003. Cerebral autoregulation during orthostatic stress in healthy controls and in patients with posturally related syncope. Clin. Auton. Res. 13, 321–329.
Cleophas, T.J., Zwinderman, A.H., 2016. Non-parametric tests for Three or more samples (friedman and kruskal-Wallis), in: Clinical Data Analysis on a Pocket Calculator. Springer, pp. 193–197.
Cohen, M.A., Taylor, J.A., 2002. Short-term cardiovascular oscillations in man: measuring and modelling the physiologies. J. Physiol. 542, 669–683. https://doi.org/10.1113/jphysiol.2002.017483
Cooke, W.H., Hoag, J.B., Crossman, A.A., Kuusela, T.A., Tahvanainen, K.U.O., Eckberg, D.L., 1999. Human responses to upright tilt: a window on central autonomic integration. J. Physiol. 517, 617–628.
Dan, D., Hoag, J.B., Ellenbogen, K.A., Wood, M.A., Eckberg, D.L., Gilligan, D.M., 2002. Cerebral blood flow velocity declines before arterial pressure in patients with orthostatic vasovagal presyncope. J. Am. Coll. Cardiol. 39, 1039–1045.
Dickinson, C.J., McCubbin, J.W., 1963. Pressor effect of increased cerebrospinal fluid pressure and vertebral artery occlusion with and without anesthesia. Circ. Res. 12, 190–202.
Dinno, A., 2015. Nonparametric pairwise multiple comparisons in independent groups using Dunn's test. Stata J. 15, 292–300.
Dwivedi, A.K., Mallawaarachchi, I., Alvarado, L.A., 2017. Analysis of small sample size studies using nonparametric bootstrap test with pooled resampling method. Stat. Med. 36, 2187–2205.
Faes, L., Erla, S., Nollo, G., 2012. Measuring connectivity in linear multivariate processes: definitions, interpretation, and practical analysis. Comput. Math. Methods Med. 2012.
Faes, L., Erla, S., Porta, A., Nollo, G., 2013a. A framework for assessing frequency domain causality in physiological time series with instantaneous effects. Philos. Trans. R. Soc. A Math. Phys. Eng. Sci. 371, 20110618.
Faes, L., Gómez-Extremera, M., Pernice, R., Carpena, P., Nollo, G., Porta, A., Bernaola-Galván, P., 2019. Comparison of methods for the assessment of nonlinearity in short-term heart rate variability under different physiopathological states. Chaos An Interdiscip. J. Nonlinear Sci. 29, 123114. https://doi.org/10.1063/1.5115506
Faes, L., Nollo, G., Porta, A., 2013b. Mechanisms of causal interaction between short-term RR interval and systolic

arterial pressure oscillations during orthostatic challenge. J. Appl. Physiol. 114, 1657–1667.
Faes, L., Pernice, R., Mijatovic, G., Antonacci, Y., Krohova, J.C., Javorka, M., Porta, A., 2021. Information Decomposition in the Frequency Domain: a New Framework to Study Cardiovascular and Cardiorespiratory Oscillations. Philos. Trans. R. Soc. A Math. Phys. Eng. Sci. in press.
Faes, L., Porta, A., Rossato, G., Adami, A., Tonon, D., Corica, A., Nollo, G., 2013c. Investigating the mechanisms of cardiovascular and cerebrovascular regulation in orthostatic syncope through an information decomposition strategy. Auton. Neurosci. Basic Clin. 178, 76–82. https://doi.org/10.1016/j.autneu.2013.02.013
Faes, L., Stramaglia, S., Marinazzo, D., 2017. On the interpretability and computational reliability of frequency-domain Granger causality. F1000Research 6.
Faes, L., Widesott, L., Del Greco, M., Antolini, R., Nollo, G., 2005. Causal cross-spectral analysis of heart rate and blood pressure variability for describing the impairment of the cardiovascular control in neurally mediated syncope. IEEE Trans. Biomed. Eng. 53, 65–73.
Force, T., 1996. Standards of measurement, physiological interpretation and clinical use. Task force of the European Society of Cardiology and the North American Society of Pacing and Electrophysiology. Circulation 93, 1043–1065.
Furlan, R., Heusser, K., Minonzio, M., Shiffer, D., Cairo, B., Tank, J., Jordan, J., Diedrich, A., Gauger, P., Zamuner, A.R., 2019. Cardiac and vascular sympathetic baroreflex control during orthostatic pre-syncope. J. Clin. Med. 8, 1434.
Furlan, R., Porta, A., Costa, F., Tank, J., Baker, L., Schiavi, R., Robertson, D., Malliani, A., Mosqueda-Garcia, R., 2000. Oscillatory patterns in sympathetic neural discharge and cardiovascular variables during orthostatic stimulus. Circulation 101, 886–892.
Gelpi, F., Bari, V., Cairo, B., De Maria, B., Tonon, D., Rossato, G., Faes, L., Porta, A., n.d. Dynamic cerebrovascular autoregulation in patients prone to postural syncope: comparison of techniques assessing the autoregulation index from spontaneous variability series. submitted.
Geweke, J., 1982. Measurement of linear dependence and feedback between multiple time series. J. Am. Stat. Assoc. 77, 304–313.
Giller, C.A., Mueller, M., 2003. Linearity and non-linearity in cerebral hemodynamics. Med. Eng. Phys. 25, 633–646.
Granger, C.W.J., 1969. Investigating causal relations by econometric models and cross-spectral methods. Econom. J. Econom. Soc. 424–438.
Grubb, B.P., Gerard, G., Roush, K., Temesy-Armos, P., Montford, P., Elliott, L., Hahn, H., Brewster, P., 1991. Cerebral vasoconstriction during head-upright tilt-induced vasovagal syncope. A paradoxic and unexpected response. Circulation 84, 1157–1164.
Guyenet, P.G., 2006. The sympathetic control of blood pressure. Nat. Rev. Neurosci. 7, 335–346.
Javorka, M., Krohova, J., Czippelova, B., Turianikova, Z., Lazarova, Z., Javorka, K., Faes, L., 2017. Basic cardiovascular variability signals: mutual directed interactions explored in the information domain. Physiol. Meas. 38, 877–894. https://doi.org/10.1088/1361-6579/aa5b77
Kapoor, W.N., 2000. Syncope. N. Engl. J. Med. 343, 1856–1862.
Krohova, J., Faes, L., Czippelova, B., Pernice, R., Turianikova, Z., Wiszt, R., Mazgutova, N., Busacca, A., Javorka, M., 2020. Vascular resistance arm of the baroreflex: Methodology and comparison with the cardiac chronotropic arm. J. Appl. Physiol. 128, 1310–1320. https://doi.org/10.1152/japplphysiol.00512.2019
Krohova, J., Faes, L., Czippelova, B., Turianikova, Z., Mazgutova, N., Pernice, R., Busacca, A., Marinazzo, D., Stramaglia, S., Javorka, M., 2019. Multiscale Information Decomposition Dissects Control Mechanisms of Heart Rate Variability at Rest and During Physiological Stress. Entropy . https://doi.org/10.3390/e21050526
La Rovere, M.T., Bigger Jr, J.T., Marcus, F.I., Mortara, A., Schwartz, P.J., Investigators, A. (Autonomic T. and R.A.M.I., 1998. Baroreflex sensitivity and heart-rate variability in prediction of total cardiac mortality after myocardial infarction. Lancet 351, 478–484.
Lassen, N.A., 1959. Cerebral blood flow and oxygen consumption in man. Physiol. Rev. 39, 183–238.
Lee, S.H., Yang, J.H., Yim, H.R., Park, J., Park, S., Park, K., On, Y.K., Kim, J.S., 2017. Hemodynamic parameters and baroreflex sensitivity during head- up tilt test in patients with neurally mediated syncope. Pacing Clin. Electrophysiol. 40, 1454–1461.

Levine, B.D., Giller, C.A., Lane, L.D., Buckey, J.C., Blomqvist, C.G., 1994. Cerebral versus systemic hemodynamics during graded orthostatic stress in humans. Circulation 90, 298–306.

Martin, K., Bates, G., Whitehouse, W.P., 2010. Transient loss of consciousness and syncope in children and young people: what you need to know. Arch. Dis. Childhood-Education Pract. 95, 66–72.

McBryde, F.D., Malpas, S.C., Paton, J.F.R., 2017. Intracranial mechanisms for preserving brain blood flow in health and disease. Acta Physiol. 219, 274–287.

Montano, N., Ruscone, T.G., Porta, A., Lombardi, F., Pagani, M., Malliani, A., 1994. Power spectrum analysis of heart rate variability to assess the changes in sympathovagal balance during graded orthostatic tilt. Circulation 90, 1826–1831.

Mosqueda-Garcia, R., Furlan, R., Fernandez-Violante, R., Desai, T., Snell, M., Jarai, Z., Ananthram, V., Robertson, R.M., Robertson, D., 1997. Sympathetic and baroreceptor reflex function in neurally mediated syncope evoked by tilt. J. Clin. Invest. 99, 2736–2744.

Nollo, G., Faes, L., Antolini, R., Porta, A., 2009. Assessing causality in normal and impaired short-term cardiovascular regulation via nonlinear prediction methods. Philos. Trans. R. Soc. A Math. Phys. Eng. Sci. 367, 1423–1440.

Nollo, G., Faes, L., Pellegrini, B., Porta, A., Antolini, R., 2000. Synchronization index for quantifying nonlinear causal coupling between RR interval and systolic arterial pressure after myocardial infarction, in: Computers in Cardiology 2000. Vol. 27 (Cat. 00CH37163). IEEE, pp. 143–146.

Nollo, G., Faes, L., Porta, A., Pellegrini, B., Ravelli, F., Del Greco, M., Disertori, M., Antolini, R., 2002. Evidence of unbalanced regulatory mechanism of heart rate and systolic pressure after acute myocardial infarction. Am. J. Physiol. - Hear. Circ. Physiol. 283, 1200–1207. https://doi.org/10.1152/ajpheart.00882.2001

Novak, P., 2016. Cerebral blood flow, heart rate, and blood pressure patterns during the tilt test in common orthostatic syndromes. Neurosci. J. 2016.

Nuzzi, D., Stramaglia, S., Javorka, M., Marinazzo, D., Porta, A., Faes, L., 2021. Extending the spectral decomposition of Granger causality to include instantaneous influences: application to the control mechanisms of heart rate variability. Philos. Trans. R. Soc. A in press.

Ocon, A.J., Kulesa, J., Clarke, D., Taneja, I., Medow, M.S., Stewart, J.M., 2009. Increased phase synchronization and decreased cerebral autoregulation during fainting in the young. Am. J. Physiol. Circ. Physiol. 297, H2084–H2095.

Panerai, R.B., White, R.P., Markus, H.S., Evans, D.H., 1998. Grading of Cerebral Dynamic Autoregulation From Spontaneous Fluctuations in Arterial Blood Pressure.

Paulson, O.B., Strandgaard, S., Edvinsson, L., 1990. Cerebral autoregulation. Cerebrovasc. Brain Metab. Rev. 2, 161–192.

Pernice, R., Sparacino, L., Nollo, G., Stivala, S., Busacca, A., Faes, L., 2021. Comparison of frequency domain measures based on spectral decomposition for spontaneous baroreflex sensitivity assessment after Acute Myocardial Infarction. Biomed. Signal Process. Control 68, 102680.

Porta, A., Bassani, T., Bari, V., Pinna, G.D., Maestri, R., Guzzetti, S., 2012. Accounting for Respiration is Necessary to Reliably Infer Granger Causality From Cardiovascular Variability Series. IEEE Trans. Biomed. Eng. 59, 832–841. https://doi.org/10.1109/TBME.2011.2180379

Porta, A., Catai, A.M., Takahashi, A.C.M., Magagnin, V., Bassani, T., Tobaldini, E., Van De Borne, P., Montano, N., 2011. Causal relationships between heart period and systolic arterial pressure during graded head-up tilt. Am. J. Physiol. Integr. Comp. Physiol. 300, R378–R386.

Porta, A., Elstad, M., 2020. Probing the cardiac arm of the baroreflex and complementary branches. Front. Neurosci. 13, 1422.

Porta, A., Faes, L., 2013. Assessing causality in brain dynamics and cardiovascular control.

Porta, A., Furlan, R., Rimoldi, O., Pagani, M., Malliani, A., Van De Borne, P., 2002. Quantifying the strength of the linear causal coupling in closed loop interacting cardiovascular variability signals. Biol. Cybern. 86, 241–251.

Porta, A., Tobaldini, E., Guzzetti, S., Furlan, R., Montano, N., Gnecchi-Ruscone, T., 2007. Assessment of cardiac autonomic modulation during graded head-up tilt by symbolic analysis of heart rate variability. Am. J. Physiol. Circ. Physiol. 293, H702–H708. https://doi.org/10.1152/ajpheart.00006.2007

Saleem, S., Teal, P.D., Howe, C.A., Tymko, M.M., Ainslie, P.N., Tzeng, Y.-C., 2018. Is the Cushing mechanism a

dynamic blood pressure-stabilizing system? Insights from Granger causality analysis of spontaneous blood pressure and cerebral blood flow. Am. J. Physiol. Integr. Comp. Physiol. 315, R484–R495.
Schiatti, L., Nollo, G., Rossato, G., Faes, L., 2015. Extended Granger causality: a new tool to identify the structure of physiological networks. Physiol. Meas. 36, 827.
Shanlin, R.J., Sole, M.J., Rahimifar, M., Tator, C.H., Factor, S.M., 1988. Increased intracranial pressure elicils hypertension, increased sympathetic activity, electrocardiographic abnormalities and myocardial damage in rats. J. Am. Coll. Cardiol. 12, 727–736.
Silvani, S., Padoan, G., Guidi, A.R., Bianchedi, G., Maresta, A., 2003. Cerebral vasoconstriction in neurally mediated syncope: relationship with type of head-up tilt test response. Ital. Hear. J. 4, 768–775.
Töyry, J.P., Kuikka, J.T., Länsimies, E.A., 1997. Regional cerebral perfusion in cardiovascular reflex syncope. Eur. J. Nucl. Med. 24, 215–218.
van Lieshout, J.J., Secher, N.H., 2008. Point: Counterpoint: Sympathetic activity does/does not influence cerebral blood flow. J. Appl. Physiol. 105, 1364–1366.
Van Lieshout, J.J., Wieling, W., Karemaker, J.M., Secher, N.H., 2003. Syncope, cerebral perfusion, and oxygenation. J. Appl. Physiol. 94, 833–848.
Voss, A., Schulz, S., Schroeder, R., Baumert, M., Caminal, P., 2009. Methods derived from nonlinear dynamics for analysing heart rate variability. Philos. Trans. Math. Phys. Eng. Sci. 277–296.
Yap, B.W., Sim, C.H., 2011. Comparisons of various types of normality tests. J. Stat. Comput. Simul. 81, 2141–2155.
Zhang, R., Zuckerman, J.H., Giller, C.A., Levine, B.D., Zuckerman, J.H., Giller, C.A., 1998a. Transfer function analysis of dynamic cerebral autoregulation in humans. Am. J. Physiol. Circ. Physiol. 274, H233–H241.
Zhang, R., Zuckerman, J.H., Levine, B.D., 1998b. Deterioration of cerebral autoregulation during orthostatic stress: insights from the frequency domain. J. Appl. Physiol. 85, 1113–1122.